A&A 671, A152 (2023)
https://doi.org/10.1051/0004-6361/202245495

Astronomy & Astrophysics

Update of the INTEGRAL/IBIS active galactic nuclei catalogue: Deeper on the Galactic plane and wider beyond

A. Malizia[1], L. Bassani[1], R. Landi[1], M. Molina[2], N. Masetti[1,3], E. Palazzi[1], G. Bruni[4], A. Bazzano[4], P. Ubertini[4], and A. J. Bird[5]

[1] OAS-Bologna, Via P. Gobetti 101, 40129 Bologna, Italy
e-mail: angela.malizia@inaf.it
[2] IASF-Milano, Via Corti 12, 20133 Milano, Italy
[3] Instituto de Astrofísica, Facultad de Ciencias Exactas, Universidad Andrés Bello, Fernández Concha 700, Las Condes, Santiago RM, Chile
[4] IAPS-Roma, Via Fosso del Cavaliere 100, 00133 Roma, Italy
[5] School of Physics and Astronomy, University of Southampton, Southampton SO17 1BJ, UK

Received 18 November 2022 / Accepted 23 January 2023

ABSTRACT

In this work we have updated the list of active galactic nuclei (AGN) detected by INTEGRAL taking into account the new objects listed in the last published INTEGRAL/IBIS survey. We have collected 83 new AGN, increasing the number of INTEGRAL-detected active galaxies (436) by 19%. Half of these new additions are located behind the Galactic plane, and for most of them we have full X-ray coverage, obtained through archival data from *Swift*/XRT, *XMM-Newton*, and *NuSTAR*. The soft X-ray data allowed us to associate each high-energy emitter with a single or multiple X-ray counterpart(s) and characterise the spectral shape of these new AGN by estimating the photon index, the intrinsic absorption, and the 2–10 keV flux. A few cases where two soft X-ray counterparts fall within the INTEGRAL error circle and at least one is classified as an AGN have been found and discussed in detail. Thirty-four sources originally listed as AGN candidates or unidentified objects have been recognised as AGN by employing three diagnostic tests: WISE colours, radio emission, and morphology. For 12 sources among the 34 AGN candidates, we reduced the optical spectra and confirmed their AGN nature, providing also their optical class and redshift. This paper is part of an ongoing effort to keep the INTEGRAL AGN catalogue updated in order to provide the scientific community with a hard X-ray selected sample of well-classified and spectrally characterised active galaxies.

Key words. X-rays: galaxies – gamma rays: galaxies – galaxies: active – galaxies: Seyfert

1. Introduction

In the past decades, the science of active galactic nuclei (AGN) has made great progress that has led to a deep knowledge of both their population in the sky and the physical mechanisms responsible for their emission over the entire electromagnetic spectrum. One of the most important results recently provided is the connection between the super massive black hole (SMBH) that powers the AGN and the host galaxy, that is, the so-called feeding and feedback cycle of active galaxies. Although the AGN-host galaxy co-evolution scenario is widely accepted and supported by clear observational evidence (Kormendy & Ho 2013; Heckman & Best 2014), there are still some issues to be addressed, mostly regarding AGN feedback (e.g., Fabian 2012). What is certain, as demonstrated by deep X-ray observations, is that most SMBHs at galaxy centres grow become increasingly hidden by dust and gas (see e.g., Hickox & Alexander 2018 for a review).

At small scales closer to the SMBH, the standard, simplistic scenario of the AGN unified model (Antonucci 1993) is now outdated. According to this theory, most of the amount of obscuring material mainly resides in the torus, which is also solely responsible for AGN classification. However, the present view of AGN is much more complex. Absorption has been revealed to be on different scales and structures, winds, outflows, and jets as well as of different natures, neutral and/or ionised (see Ramos Almeida & Ricci 2017 for a review). As for the absorbing torus itself, its structure (Zhao et al. 2021) and its connection to its surroundings (e.g., Netzer 2015) are not yet well understood.

Therefore, absorption is shown to be a fundamental key for understanding both the geometry of the innermost part of the AGN and the feedback with the host galaxy. The most efficient way to study absorption and address these still open issues is to have large samples of AGN selected in the hard X-ray band (>20 keV), which is far less biased towards absorption. Since the early 2000 s, both INTEGRAL/IBIS (Ubertini et al. 2003) and *Swift*/BAT (Barthelmy et al. 2005), thanks to their good sensitivity and wide-field sky coverage in the high-energy domain (14–200 keV), have provided a remarkable improvement in our knowledge of the high-energy extragalactic sky by detecting more than 2000 (mostly local) AGN. It is worth noting that due to its observational strategy, *Swift*/BAT performs a nearly uniform all-sky survey, and so it is more effective at higher Galactic latitudes. INTEGRAL, on the other hand, provides a sky survey with exposures that are deeper in the Galactic plane and Galactic centre regions. INTEGRAL also has a higher angular resolution, which is essential in these crowded regions. These characteristics make the two observatories fully complementary in the case of extragalactic studies.

INTEGRAL surveys were particularly important in detecting highly absorbed AGN along the Galactic plane. The area

comprised between ±10–15 degrees above and below the Galactic plane, the so-called zone of avoidance, is rich with gas and dust, which obscure starlight and screen nearly all background extragalactic objects from traditional optical-wavelength surveys (in the optical, as much as 20% of the extragalactic sky is obscured by the Galaxy). As a consequence, the Galactic plane was historically not a focus for extragalactic astronomy. Before the advent of INTEGRAL since hard X-rays (>10 keV) are able to penetrate this zone, providing a window that is virtually free of obscuration relative to optical wavelengths and partly to soft X-rays. The capabilities of INTEGRAL/IBIS in studying extragalactic sources were revealed soon after the launch of the satellite, and it soon became evident that the population of AGN emitting above 20 keV was growing thanks to the discovery that many of the new hard X-ray detected sources (IGR sources) were indeed active galaxies. In the first IBIS survey (Bird et al. 2004), based on the first year of INTEGRAL observations, there were only five AGN listed, and this number became 33 (almost 20% of the entire catalogue) in the second survey (Bird et al. 2006). Since 2004, a sequence of IBIS all-sky survey catalogues (Bird et al. 2016 and references therein) as well as deep surveys of the Galactic centre region and Galactic plane (Revnivtsev et al. 2004, 2006; Krivonos et al. 2007, 2012, 2017) have been published at regular intervals, making use of an ever increasing dataset. As the total number of known or newly discovered AGN grew, it was possible to assemble them for population studies, as has been done over the years (Malizia et al. 2012, 2016, 2020a). So far, the number of AGN listed in this dataset amounts to 436 objects.

Taking advantage of the hard X-ray selection, this now large sample of AGN has been exploited to carry out several studies on relevant issues of extragalactic science, such as the possibility to identify highly obscured AGN (e.g., Compton thick sources) more easily (Malizia et al. 2007). This sample has also allowed for more precise constraints on the absorption properties of the local AGN population and led to the finding that the true fraction of Compton thick AGN is ~20%of the sample population (Malizia et al. 2009b). Furthermore, broadband spectral (0.2–100 keV) analysis of a complete sample of Seyfert 1 galaxies allowed Malizia et al. (2014) to constrain for the first time the value of the high-energy cut-off at around 100 keV, clearly indicating that the primary continuum typically decays at much lower energies than previously thought. Alongside INTEGRAL, *Swift*/BAT has also contributed to these topics, mostly by confirming INTEGRAL results (Burlon et al. 2011; Ricci et al. 2015, 2017; Kamraj et al. 2022).

Given the scientific relevance of the above results, it is fundamental to keep updating the AGN high-energy catalogues. The last INTEGRAL all-sky survey by Krivonos et al. (2022) collects all the INTEGRAL observations from over 17 years until January 2020 and lists 929 hard X-ray sources detected above the 4.5σ threshold, of which 113 are reported as unclassified. In this work, in order to update the catalogue of INTEGRAL AGN, we have added the AGN from Krivonos' list that have not been reported as being previously detected by INTEGRAL. We have also searched for the soft X-ray counterparts of these AGN in order to study their spectral behaviour. Moreover, we have tried to pinpoint the unidentified sources listed in Krivonos et al. (2022) that are likely to be AGN on the basis of diagnostic indicators such as WISE colours, radio emission, and indication of extension in the optical images. Finally, we have also classified 12 of the AGN candidates by analysing their optical spectra.

2. New AGN: The sample

The aim of this work is to update the list of AGN detected by INTEGRAL while taking into account the new active galaxies already listed in the Krivonos et al. (2022) survey. We collected 83 new AGN, listed in Table A.1. Among these, four sources have already been listed in Malizia et al. (2016) as AGN candidates and were re-analysed in this work in order to be optically classified. The three objects highlighted in bold in Table A.1, are from Bird et al. (2016); 34 objects are unclassified AGN, of which 22 have been already proposed as AGN candidates; and the rest, 12, are unidentified objects in the Krivonos et al. (2022) survey and have been classified or are proposed as AGN in the present work (see Sect. 4). In Fig. 1, the entire INTEGRAL AGN sample collected so far is shown with the different classes differentiated. The last additions have been highlighted with filled symbols. As clearly seen from Fig. 1, the new AGN collected in this work reside well within the parameter space of the INTEGRAL AGN sample (see AGN review by Malizia et al. 2020b), but it is worthy to note that a large fraction of the new AGN are located on the Galactic plane. In Fig. 2, the entire sample of INTEGRAL AGN is plotted in the sky, including the AGN reported in previous catalogues (Malizia et al. 2020a, 2016, 2012) and the 83 AGN collected in this work. It is evident that a large number of the new additions are located in the plane of the Galaxy, as 43% of the sample are within ±10 degrees above and below the Galactic plane. The percentage rises to almost half of the sample when within ±15 degrees.

We were able to obtain full X-ray coverage of almost the entire sample by making use of data from *Swift*/XRT, *XMM-Newton*, and *NuSTAR* archives. Only two objects, IGR J06380-7536 and RX J1317.0+3735, had no 2–10 keV data available. Instead, there was only a soft X-ray flux from the XMM Slew Survey (Saxton et al. 2008). The 2–10 keV data were used to associate the high-energy emitter with a single or multiple X-ray counterpart(s), providing a better (arcsec) position. For the counterpart search, we adopted the positional uncertainties cited by Krivonos et al. (2007) (see next section). Hard, bright X-ray sources were favoured over soft, dim objects. The soft X-ray data were also used to characterise the high-energy source at low energies. Unfortunately, in most cases, the statistical quality of the 2–10 keV data is poor, and therefore we employed a simple model consisting of an absorbed power law that allowed us to estimate the main spectral parameters, such as the intrinsic absorption[1] and the 2–10 keV flux (e.g., Malizia et al. 2016).

In Table A.1 we list the new AGN together with their essential information, as always reported in our catalogues, including: alternative names (Col. 2); the most precise coordinates RA and Dec (Cols. 3 and 4); whether from optical or soft X-rays (*Chandra* or *Swift*/XRT); redshift (Col. 5); and optical class, taken from NED, Simbad archives, or Véron-Cetty & Véron (2010) (Col. 6). The X-ray spectral parameters reported in this work are column density, photon index, and 2–10 keV flux (Cols. 7–9). The hard X-ray flux (20–100 keV, Col. 9) was extrapolated from Krivonos et al. (2022). In Col. 11, the references for the 2–10 keV spectral parameters are given for sources already published in the literature.

3. Cases with multiple counterparts

In this new sample of AGN detected by INTEGRAL, we have found a few cases where two soft X-ray counterparts fall within

[1] Our approach always considered the Galactic absorption in spectral fitting.

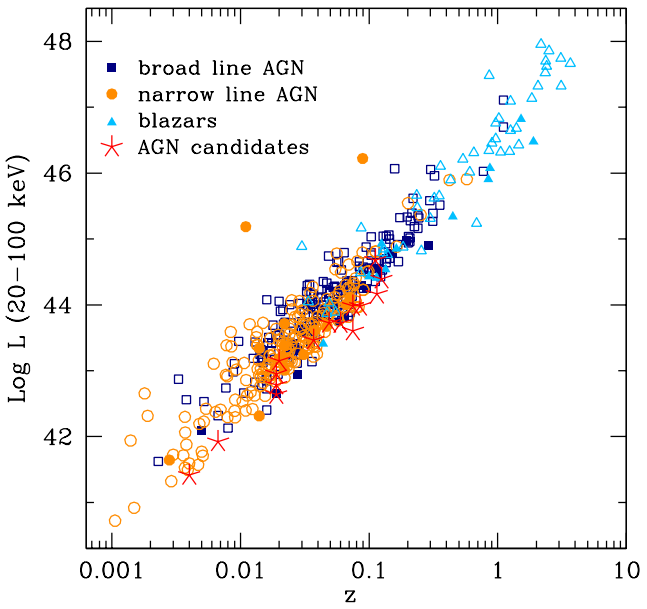

Fig. 1. Observed hard X-ray (20–100 keV) luminosity versus redshift for whole INTEGRAL AGN sample. Blue squares are broad-line AGN, gold circles are narrow line AGN, and light blue triangles are blazars. Red stars are AGN candidates still unclassified for which a measure of redshift is available. The filled symbols refer to the new AGN added in this work.

the INTEGRAL error circle and at least one is classified as an AGN. These objects are discussed individually in the following sub-sections. In this work, following Krivonos et al. (2007), we used a 4.2 arcmin search radius (90% confidence level for a source detected at five to six standard deviations). In cases where there was no detection of a counterpart, we used a 6.5 arcmin (99%) to search for possible X-ray counterparts. Only counterparts coincident with well-defined, active galaxies are reported in Table A.1, and other potential associations are briefly described in this section. In the Appendix we show the *Swift*/XRT 0.3–10 keV images of sources discussed below. We note that in cases where both sources were detected above 3 keV, the hard X-ray emission detected by INTEGRAL and reported in Krivonos et al. (2022) was considered as the combination of the two sources. Therefore in Col. 9 of Table A.1, only estimates of 20–100 keV fluxes have been provided.

3.1. IGR J04288-6702 also SWIFT J0428.2-6704 A/B

In the case of IGR J04288-6702 (see Fig. B.1, left panel), we found two objects emitting above 3 keV. Both of the objects are outside the 90% but inside the 99% IBIS positional uncertainty. One object (#1) is the Seyfert 1.5 galaxy LEDA 299570, reported in Table A.1 and also reported in Krivonos et al. (2022), while the other object (#2), at ∼11.5 arcmin, is the Galactic source SXPS J042749.2-670434 (RA(J2000) = 04 27 49.63, Dec(J2000) = −67 04 34.8), also reported as a *Fermi*/LAT source, 4FGL J0427.8-6704 (see Fig. B.1, left panel). The latter object is associated with an eclipsing low-mass X-ray binary (P = 8.8 h) with a main-sequence donor and a neutron-star accretor (Strader et al. 2016; Marchesini et al. 2020). The X-ray light curve also shows properties similar to those seen among known transitional millisecond pulsars: short-term variability, a hard power-law spectrum ($\Gamma \sim 1.7$), and a comparable 0.5–10 keV luminosity ($2.4{\times}10^{33}$ erg s^{-1}). Furthermore, the source is remarkable for its face-on inclination in the range of 5–8°, depending on the neutron star and donor mass (Britt et al. 2017). Moreover, a gamma-ray eclipse having the same phase as the optical one has been recently reported together with an X-ray eclipse (Kennedy et al. 2020). This is clearly a very interesting object that deserves further study, especially in the hard X-ray band. *NuSTAR*, having an angular resolution better than IBIS, can allow for discrimination and study of these two sources.

3.2. PKS 0440-00 and 1RXS J044229.8-001823

In the right panel of Fig. B.1, we show a very peculiar case where two blazars fall within the IBIS error circle: PKS J044-00, a flat-spectrum radio quasar at z = 0.845, also known as QSO B0440-003 (#1 in Fig. B.1), and 1RXS J044229.8-001823, a BL Lac object at z = 0.449, also known as 2MASS J04423023-0018294 (#2 in Fig. B.1). Because there are two AGN in the IBIS error circle, it is incorrect to quote PKS 0044-00 as the only INTEGRAL detection as listed in Krivonos et al. (2022) survey catalogue, and we suggest instead that this source be called IGR J04426-0018 since its emission is the merger of two objects. The QSO was also detected up to the GeV band by *Fermi*/LAT and reported as 4FGL J0442.6-0017 (Ajello et al. 2020) in the fourth AGN catalogue. Regarding the BL Lac, it was originally indicated in the third *Fermi* catalogue as a possible counterpart, but it has been excluded in latest one. The BL Lac object is listed in the 3HSP catalogue of high synchrotron-peaked blazars (Chang et al. 2019), showing a synchrotron peak at around $2{\times}10^{16}$ Hz. To estimate the 20–100 keV flux of each source, we assumed an equal share of emission as implied by the almost equal flux at soft X-ray energies and a similar spectral shape at X-ray energies. This would also be an interesting sky field to be observed by the *NuSTAR* telescope.

3.3. SWIFT J0835.5-0902

As evident in the XRT image shown in Fig. B.2 (left panel), in this field too we found two hard X-ray emitters associated with a single INTEGRAL/BAT source, although a unique identification is provided in the 157-month *Swift*/BAT catalogue (Oh et al. 2018). The first object (#1 in Fig. B.2), which is also reported in Table A.1, is located at RA(J2000) = 08 35 33.34 and Dec(J2000) = 09 05 30.2 (3.5 arcsec X-ray positional uncertainty), and it is associated with the extended infrared object 2MASX J08353333-0905302. This galaxy (i.e. object #1) is reported in Simbad with no redshift, while NED provides a photometric redshift of z = 0.1124. The object's WISE colours, $W1 - W2$ = 0.86 and $W2 - W3$ = 2.87, are typical of AGN (Secrest et al. 2015). The object is listed as a source in the UV-bright QSO survey of Monroe et al. (2016), and it is also identified with an active galaxy from multi-waveband analysis (Edelson & Malkan 2012). The lack of intrinsic absorption in the X-ray spectrum indicates that this is most likely a broad-line AGN.

The other object (#2 in Fig. B.2), located at RA(J2000) = 08 35 31.5 and Dec(J2000) = −09 04 18.6 (3.8 arcsec X-ray positional uncertainty), is a Galactic source. It is also reported as an XMM Slew source with 0.2–12 keV flux in the range 2.4–$3.6{\times}10^{-12}$ erg cm^{-2} s^{-1}. The XRT spectrum is well fitted by a power law with a photon index of 1.24±0.27 and a 2–10/0.2–12 keV flux of $8.1{\times}10^{-13}$/$1.2{\times}10^{-12}$ erg cm^{-2} s^{-1}, which is lower

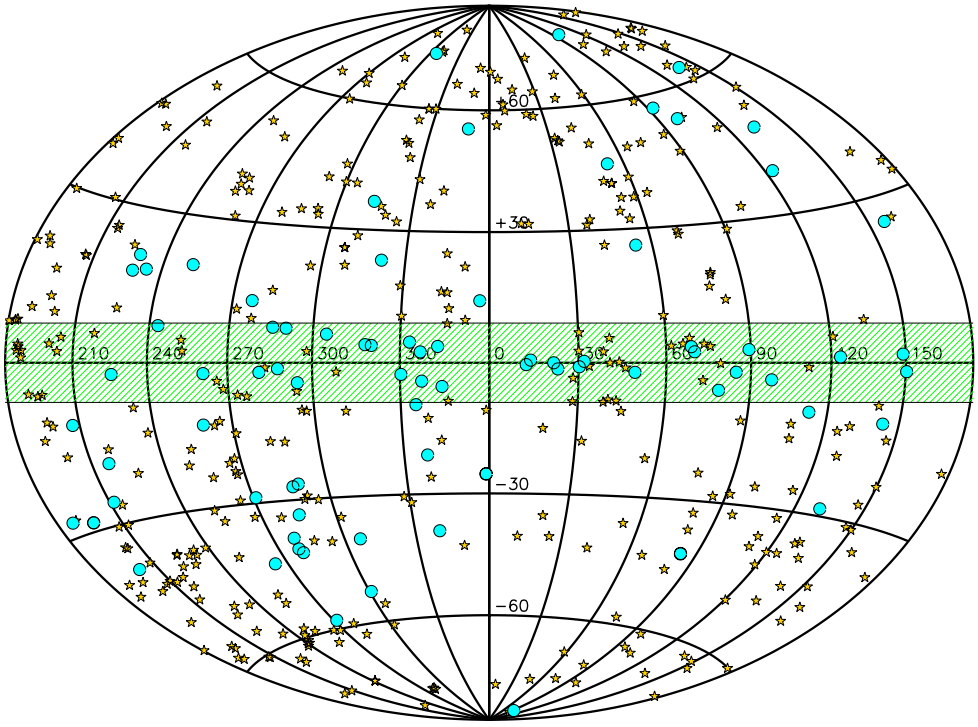

Fig. 2. All the AGN detected so far by INTEGRAL/IBIS plotted on the sky. The circles represent the 83 new active galaxies studied in this work, while the stars are the AGN detected in previous surveys and reported in Malizia et al. (2012, 2016, 2020a).

than that measured by *XMM-Newton*. The source is associated with the variable star ASAS J083531-0904.1[2] and classified as a rotating variable at a distance of 4.3 Kpc (*Gaia* parallax) with a possible period of 171.2 days. However, it is worth noting that in the *Gaia* colours versus absolute magnitude diagram (BP-RP = 2.1; absolute magnitude = −1.83), the source is located in the region populated by eclipsing binaries. It would be interesting to study this source further in order to unveil its true nature and its contribution to the overall IBIS emission.

3.4. IGR J12418+7805

Another interesting case is IGR J12418+7805, where possibly two objects contribute to the overall emission seen by INTEGRAL; unfortunately, no *Swift*/XRT observation is available. We found one source lying within the IBIS error circle, and it is clearly reported as an X-ray emitter both in the ROSAT Bright Source (Voges et al. 1996) and in the XMM Slew Survey (Saxton et al. 2008), and it is therefore listed in Table A.1. The source is associated with the galaxy LEDA 140000 at a redshift of $z = 0.022$, which is classified as a Seyfert 1.9 in the Véron-Cetty & Véron (2010) catalogue and has a 0.2–12 keV flux of 2.1×10^{-12} erg cm^{-2} s^{-1}. Assuming a typical value 1.8 for the power law photon index, we have extrapolated the 2–10 keV flux value reported in Table A.1.

The second source, reported only in the XMM Slew Survey catalogue, is at ∼2.2 arcmin distance from the previous one and is located at RA(J2000) = 12 43 13.8, Dec(J2000) = +78 08 28, with an associated positional uncertainty of ∼10 arcsec. It is brighter than LEDA140000, with a 0.2–12 keV flux of 6×10^{-12} erg cm^{-2} s^{-1}. The source class is unclear, although its location at high-galactic latitude suggests an extragalactic nature. The two XMM Slew sources were detected at different epochs (almost one year apart), and no radio, infrared, nor optical association could be found within the XMM Slew positional uncertainty of the second source. Only by enlarging its positional uncertainty to 15 arcsec is it possible to find a WISE source with $W1 - W2 = 0.47$ and $W2 - W3 = 4.04$, which are more typical of starburst galaxies than AGN (Jarrett et al. 2017). Due to these uncertainties, we decided not to list this second source amongst the current INTEGRAL AGN update, as we prefer to wait for a more sensitive hard X-ray image of this sky region to confirm its contribution to the overall INTEGRAL emission.

3.5. SWIFT J1937.5-4021

SWIFT J1937.5-4021 is reported as an unidentified object in the Krivonos et al. (2022) list, but we found that the most likely soft X-ray counterpart for both IBIS and BAT detection is the XRT source located at RA(J2000) = 19 37 13.47 and Dec(J2000) = −40 16 14.84 (3.6 arcsec error radius), detected at 27σ in the 0.3–10 keV band (20σ above 3 keV) and well inside the IBIS error circle (see source #1 in Fig. B.2, left panel). This X-ray source is also reported as an XMM Slew source with a 0.2–12 keV flux of 1.37×10^{-12} erg cm^{-2} s^{-1} and associated with the galaxy LEDA 588288 with $z = 0.075$ in the Simbad archive but reported in NED with a photometric redshift of $z = 0.055776$. Our analysis of the X-shooter optical spectrum of this source allowed us to confirm its nature, classifying it as a Seyfert 2 galaxy and measuring its true redshift of $z = 0.0193$ (see Sect. 4.2).

The other possible counterpart, although outside the 90% but inside the 99% IBIS error circle, is associated with the ROSAT source 1RXS J193716.1-401026 and is located at RA(J2000) = 19 37 14.70 and Dec(J2000) = −40 10 14.91 (3.64 arcsec positional uncertainty). *Swift*/XRT detected this source at 23σ in the 0.3–10 keV band (9σ above 3 keV). As evident from Fig. B.2 (right panel) both sources are well inside

[2] https://www.aavso.org/vsx/index.php?view=detail.top&oid=281217

the 90% BAT error circle. We suggest an extragalactic origin for 1RXS J193716.1-401026 since *Gaia* does not detect a significant parallax or proper motion (Liao et al. 2019). Moreover, its observed WISE colours (see Sect. 4.1) are typical of AGN. Both XRT detections are hard X-ray sources, confirming that both can contribute to the high-energy emission seen by IBIS.

3.6. AX J2254.3+1146 also SWIFT J2254.2+1147 A/B

This is another case where two AGN fall within the IBIS positional uncertainty, although one is well inside the error circle, while the other is just at its border but inside the 99% error circle (see Fig. B.3). Both sources are well detected above 3 keV. They have similar redshifts, but no interaction is evident between the two. The first object, UGC 12237 (#1 in Fig. B.3), is a Seyfert 2 galaxy, while the second object is a Seyfert 1 (UGC 12243; #2 in Fig. B.3), according to Véron-Cetty & Véron (2010). Both AGN are hosted in edge-on galaxies of 0.24 and 0.34 axial ratio (major over minor axis), respectively. This is also an interesting set of sources to be observed with the *NuSTAR* observatory in order to study both AGN, as already done for IGR J16058-7253 (Molina et al. 2021).

4. Unclassified objects

Thirty-four sources (~41% of the total sample) listed in Table A.1 are unclassified AGN. Of these sources, 22 were already identified as active galaxies in the Krivonos et al. (2022) survey, while the remaining 12 are reported as unidentified sources and proposed as AGN candidates in this work. For this set of 34 sources, we investigated their AGN nature by means of a two-step approach. First, we used multi-waveband information to assess their nature. In particular, we made use of three diagnostics to confirm their nuclear activity: WISE colours, detection of radio emission, and other extragalactic features, such as location in the sky, measured redshift, and optical morphology (i.e. we have searched for indication of extension in their optical and/or near-IR images). In the second step, we searched public archives for optical spectra of these unclassified sources, finding that 40% of the sample indeed had public data. The results of this two-step approach are presented in the following sections.

4.1. Multiwaveband AGN signature: WISE colours, radio emission, and other features

It is now well established that WISE colours $W1-W2$ and $W2-W3$ can be used to select AGN, or more specifically, efficiently accreting objects. AGN are typically located in a well-defined region of the WISE colour-colour diagram (i.e. in a region limited by $W1-W2>0.5$ and $2<W2-W3<5.1$; see Secrest et al. 2015 for more details on the boundary delimitation). We therefore collected WISE colours for all of the unclassified objects in order to confirm their extragalactic nature. For this task, we used the ALLWISE catalogue (Mainzer et al. 2014), which contains accurate positions, apparent motion measurements, four-band fluxes, and flux variability statistics for over 747 million objects detected on the co-added Atlas Images. For only one source (IGR J19577+3339) not reported in the ALLWISE database, we used the CatWISE2020 catalogue (Marocco et al. 2021), which lists only $W1$ and $W2$ magnitudes and thus provides only one infrared colour. Table 1 lists the WISE colours of all unclassified sources, while Fig. 3 shows the corresponding positions in the WISE colour-colour diagram.

Apart from the WISE colours, indication for the presence of an active nucleus also comes from radio emission since almost all AGN detected by INTEGRAL so far have a radio counterpart, which is not necessarily radio loud but can emit at a level of a few mJy. We therefore investigated the radio properties of the unidentified objects using as a first step radio catalogues of old surveys. Specifically, for data at 1.4 GHz we used the National Radio Astronomy Observatory's Very Large Array Sky Survey (NVSS, Condon et al. 1998) and the Multi-Array Galactic Plane Imaging Survey (MAGPIS, Helfand et al. 2006), while for data at 0.83 GHz, we used the Sydney University Molonglo Sky Survey (SUMSS, Mauch et al. 2003) and the Molonglo Galactic Plane Survey 2nd Epoch (MGPS-2, Murphy et al. 2007). These surveys are similar in sensitivity and spatial resolution and together cover the whole sky, making them particularly well suited for searching radio emission from our unclassified objects. However, since their sensitivity threshold is around the 10 mJy level, a number of sources dimmer than this flux could not be detected. In these cases, we consulted more recent all-sky surveys, such as the VLA Sky Survey (VLASS, Gordon et al. 2021) at 3 GHz and the Rapid ASKAP Continuum Survey (RACS, McConnell et al. 2020) at 0.88 GHz. The radio fluxes obtained from all of these surveys are listed in Table 1, which also specifies the database used. The data in Table 1 also indicate that most objects are radio emitters, and although the majority have relatively weak fluxes, this nonetheless confirms the presence of an active nucleus at their centres. At the resolution of the surveys employed, most of these detections correspond to a compact and single component morphology, except for four objects (displayed in Figs. C.1 and C.2) that show a more complex radio shape.

Finally, we adopted other extragalactic indicators, such as the knowledge of the source redshift, the location above or below the Galactic plane, or the presence of extended emission typical of a galaxy morphology. The evidence of source extension was obtained from inspection of optical and near-IR images provided by the Dark Energy Camera Plane Survey (DECaPS, Schlafly et al. 2018), which is the most suitable for our sources because it surveys the Galactic plane. A note related to the presence of a redshift or of extension in optical images as well as an indication of the source location with respect the Galactic plane is reported in the last column of Table 1. In order to validate our AGN selection and definitively classify a source as an AGN, we adopted the criterion that at least two of the three diagnostics used have to be satisfied.

As clearly shown in Fig. 3, WISE colour values point to an AGN nature for the majority of the objects except for seven of them, which are characterised by $W1-W2$ colours below the 0.5 line and $W2-W3$ colours below the two threshold, as adopted by Secrest et al. (2015). Five of the six sources with values below the $W1-W2$ colour threshold (IGR J03574-6602, IGR J06075-6148, IGR J06503-7742, IGR J16459-2325, and IGR J17255-4509) are however associated with galaxies with a measured redshift, while the only exception, IGR J16246-4556, is extended in the DECaPS image. The only source above the $W1-W2=0.5$ line and outside the $W2-W3=2$ boundary (although only marginally so), is AX J1830.6-1002, which is a very puzzling case. As pointed out by Bassani et al. (2009), AX J1830.6-1002 is an AGN located in the Galactic plane inside a diffuse radio supernova remnant. It is spatially coincident with a compact radio source that has an X-ray spectrum typical of a Compton thick AGN. Given the complexity of its local

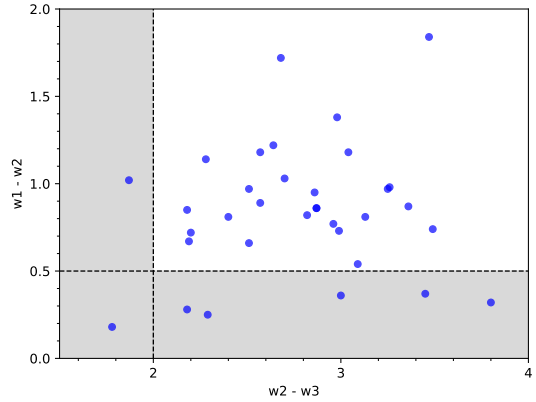

Fig. 3. WISE colour-colour diagram of 34 AGN candidates. The lines from Secrest et al. (2015) delimit the area populated by AGN. Six sources (IGR J03574-6602, IGR J06075-6148, IGR J06503-7742, IGR J16246-4556, IGR J16459-2325, and IGR J17255-4509) have low $W1 - W2$ values and need to be investigated further. The only source with $W2 - W3$ below two is AX J 1830.6-1002, which is a very peculiar case.

environment and considering the uncertainties associated with the WISE magnitudes, we do not consider this source an outlier. Furthermore, it is worth noting that six of these seven sources have radio detection, with the exception being IGR J16459-2325, as only a RACS upper limit is available.

According to Secrest et al. (2015), the number of contaminating stellar objects in their mid-IR AGN sample is very small, below 0.04%, making their selection extremely reliable. Moreover, they cite their sample completeness to be ∼84%, meaning that 16% of AGN are not selected using their method mainly because they display a $W1 - W2$ colour bluer than allowed (i.e. below the 0.5 line). Interestingly, this is very close to the percentage of AGN (18%) we found below $W1 - W2 = 0.5$ both in the present sample and when considering the entire set of INTEGRAL AGN, where 507 out of 519 objects are listed in the ALLWISE catalogue. The unusual WISE colours are generally associated with heavily absorbed AGN, as pointed out by Gandhi et al. (2015), or with low luminosity AGN, for example radiatively inefficient accretors, such as LINERs, as indicated by (Mingo et al. 2016). In objects classified as LINERs, the host galaxy dominates the mid-IR emission with respect to the AGN, moving them below the 0.5 threshold in the $W1 - W2$ versus $W2 - W3$ diagram (Herpich et al. 2016)[3].

As can be seen from Table A.1, the X-ray column densities of our six outliers indicate that four out of six objects are indeed absorbed with $N_{\rm H}$ in excess of 10^{23} cm^{-2}, suggesting that the first hypothesis is a viable explanation for their unusual WISE colours. However, as discussed in Sect. 4.2, the low luminosity AGN possibility turns out to be an equally valid argument.

As evident from the values reported in Table 1, nearly all of our AGN candidates have radio detections. Five sources (IGR J04085-6546, IGR J14417-5533, IGR J16459-2325, SWIFT J1839.1-5717, and SWIFT J1937.5-4021) were not detected in the radio band, and for these sources, we were able to extract only upper limits from RACS images. Nevertheless, for all five of these sources, WISE colours and morphology features point to an extragalactic nature, and therefore, we are reasonably confident that our final AGN selection is correct (see also following section).

It is worth noting that the radio data analysis performed in this work was crucial in unveiling the AGN nature of several objects, and such is the case for IGR J19577+3339. This source is the only one with just one WISE colour and no other diagnostic indicator of being extragalactic. As clearly shown in the left panel of Fig. C.1, IGR J19577+3339 is a strong radio emitter that is used in the literature as a flat-spectrum radio quasar calibrator (Charlot et al. 2020). A central bright component is visible in VLASS with some additional emission at about 5 arcsec towards NE and SW, most probably not correlated with the source. Previous VLBI studies at 2.3 and 8.6 GHz (Pushkarev & Kovalev 2012) showed a bent jet on the pc-scale.

Another source for which the radio detection and radio morphology is decisive in assessing its AGN nature is IGR J08297-4250. As shown in Fig. C.1 (right panel), the source shows a core plus jet-like structure in RACS, reminiscent of a blazar source, although at a relatively low radio flux.

Finally, we note that two additional objects, PKS 1413-36 and IGR J16005-4645, show strong radio fluxes above the 1 Jy level. The first object is associated with a radio galaxy of a large size (around 430 kpc; see Fig. C.2, left panel), while the second object is so far still morphologically unclassified (although it is reported as extended in some surveys, such as ATCA; McConnell et al. 2012) and poorly studied at radio frequencies. The RACS image of IGR J16005-4645 (see Fig. C.2, right panel) shows a core plus jet-like structure, but, combining data from various surveys, the radio spectrum is steep (−0.7/−1) over the entire 0.150–20 GHz range. This suggests a large viewing angle and a possible radio galaxy morphology with a lobe pointing towards our point of observation. We also note that the radio and X-ray positions are displaced by roughly 28 arcsec. This discrepancy could be interpreted as a radio galaxy where the radio position refers to one of the two lobes, while the X-ray position coincides with the source core. Alternatively, one must assume that the radio object is instead composed of two sources not fully resolved in the radio image and associated with different optical counterparts. Indeed, the radio central position is compatible within errors with one weak *Gaia* EDR3 catalogue source (2020 VizieR On-line Data Catalog: I/350) of unknown class. In any case, the X-ray source, actually the secure counterpart of the INTEGRAL emitter, is likely an AGN not only on the basis of its WISE colours and possible radio emission, but also according to the SIX index developed by Edelson & Malkan (2012). This index was empirically constructed by combing infrared colours over the 2–10 micron waveband (to ensure an AGN-like continuum) and the distance to the nearest X-ray source. A value below zero of the resulting SIX index (−0.258 in our case) indicates an object with a high likelihood (greater than 95%) of being an AGN.

4.2. Optical spectroscopy

For 12 sources, amongst the sample of 34 AGN candidates, we acquired reduced optical spectra available from the 6dF[4], PESSTO[5], and X-shooter[6] databases and then analysed the

[3] Of the 29 Compton thick AGN and 19 LINERs (or Seyfert/LINERs) present in the entire AGN sample, 12 (41%) of the first and ten (53%) of the second are located below the $W1 - W2 = 0.5$ line, suggesting that these two types of active nuclei have a far greater chance than other AGN types to fall below the adopted threshold.

[4] Available at: http://www-wfau.roe.ac.uk/6dFGS/form.html

[5] Available at: https://www.eso.org/qi/catalogQuery/index/365

[6] Available at: http://archive.eso.org/eso/eso_archive_main.html

Table 1. AGN candidates.

Source	WISE colours		RADIO FLUX			Extra Data
	$W1-W2$	$W2-W3$	SUMSS (0.843GHz)	NVSS (1.4GHz)	Other	AGN marks
IGR J03574-6602	0.32	3.80	16.8±1.7	–	–	z
IGR J04059+5416	0.82	2.82	–	–	1.92±0.30 [(a)]	–
IGR J04085-6546	0.72	2.20	–	–	<33.0 [(c)]	z
IGR J06075-6148	0.37	3.45	52.3±3.6	–	–	z
IGR J06503-7742	0.25	2.29	–	–	5.10±0.51 [(c)]	z
IGR J08297-4250	0.54	3.09	–	–	4.81±0.48 [(c)]	Ext
SWIFT J0835.5-0902	0.86	2.87	–	–	2.88±0.29 [(c)]	z
SWIFT J0958.2-5732	1.14	2.28	13.2±1.9	–	–	z
IGR J11275-5319	0.97	3.25	14.0±1.1	–	–	z
IGR J11299-6557	1.18	3.04	–	–	5.98±0.60 [(c)]	–
IGR J13045-5630	0.98	3.26	16.8±1.4	–	–	–
PKS 1413-36	1.03	2.70	–	1098.2±34.3	–	z
IGR J14417-5533	0.97	2.51	–	–	<0.84 [(c)]	Ext
IGR J14557-5448	0.81	3.13	33.1±1.4	–	–	–
IGR J16005-4645	1.22	2.64	7843.0±235.3	–	–	–
IGR J16181-5407	1.18	2.57	–	–	10.5±1.00 [(c)]	z
IGR J16246-4556	0.18	1.78	–	–	9.51±0.95 [(c)]	Ext
IGR J16413-4046	0.95	2.86	–	–	2.23±0.22 [(c)]	–
IGR J16459-2325	0.28	2.18	–	–	<0.99 [(c)]	z
IGR J16560-4958	0.67	2.19	–	–	11.4±1.14 [(c)]	Ext
IGR J17157-5449	0.86	2.87	–	–	7.09±0.71 [(c)]	–
IGR J17255-4509	0.36	3.00	10.9±1.2	–	–	z
IGR J18134-1636	0.74	3.49	–	–	1.98±0.40 [(a)]	–
IGR J18141-1823	0.73	2.99	–	–	10.3±6.80 [(b)]	–
AXJ 1830.6-1002	1.02	1.87	–	–	2.54±0.40 [(a)]	–
SWIFT J1839.1-5717	1.84	3.47	–	–	<0.57 [(c)]	$l \leq -20$
IGR J18486-0047	1.72	2.68	–	20.6±1.7	–	–
IGR J18497-0248	0.66	2.51	–	15.9±1.6	–	–
IGR J19294+1328	0.89	2.57	–	–	3.42±0.30 [(a)]	–
SWIFT J1937.5-4021-1	0.77	2.96	–	–	4.87±0.49 [(c)]	z
SWIFT J1937.5-4021-2	0.81	2.40	–	–	<1.05 [(c)]	$l \leq -20$
IGR J19504+3319	0.85	2.18	–	–	3.972±0.2 [(a)]	–
IGR J19577+3339	0.8*	–	–	295.2±8.9	–	–
SWIFT J2055.0+3559	1.38	2.98	–	9.6±0.5	–	z

Notes. [(a)]VLASS; [(b)]MAGPIS; [(c)]RACS.

collected data using IRAF 4[7]. Regarding IGR J17255-4509, SWIFT J1839.1-5717, and SWIFT J1937.5-4021, we stacked together the different spectra to increase the signal-to-noise ratio (S/N). As a result, we found that except for IGR J04085-6546, IGR J08297-4250, and SWIFT J1839.1-5717, all sources show optical features that are typical of AGN. In order to provide a classification for these 12 objects, we examined the diagnostic ratio ([OIII]λ5007/H$_\beta$ and [NII]λ6583/H$_\alpha$) according to Ho et al. (1993) and Kauffmann et al. (2003). The results of our findings are reported in Table 2, where we list the instrument used for the optical observation, the line ratios used to determine the class, the measured redshift, and AGN class for each source. In this work, we report for the first time the optical class of nine objects and the redshift values for three sources, namely, IGR J11275-5319, IGR J13045-5630, and IGR J16560-4958 (see Table 2). For the remaining six galaxies classified in this work, the redshifts we estimated are compatible with the values in the literature. Of the nine sources with a clear optical class, four are LINERs and five are type 2 AGN. Interestingly, all four LINERs fall below the AGN threshold line of 0.5 in the WISE colour-colour diagram (Fig. 3). As mentioned before, although a contribution from absorption cannot be excluded, the low values could indicate that the unusual WISE colours are due to radiatively inefficient accretion typically associated with such low luminosity objects as LINERs. As further proof of this possibility, we note that NGC 4102, the only other LINER object in our sample, also has WISE colours ($W1-W2 = 0.37$ and $W2-W3 = 4.1$) that locate it in the same region of the diagram. On the other hand, this suggests that IGR J16246-4556 and IGR J16459-2325 could be also LINERs, as they are located below the AGN threshold in the WISE diagram of Fig. 3. Unfortunately, there is no optical spectrum available for them. Most of these LINERs are of type 2, with the possible exception of IGR J17255-4509, where a broad HeI line has been detected in the near-IR spectrum (Ricci et al. 2022), and indeed they are absorbed in X-rays, except for IGR J17255-4509.

[7] https://iraf-community.github.io

Table 2. Confirmed AGN: Optical spectra.

Source	Instrument	Log(OIIIλ5007/H$_\beta$)	Log(NIIλ6583/H$_\alpha$)	H$_\alpha$/H$_\beta$	z	Class
IGR J03574-6602	X-shooter	0.42	−0.120	5.73	0.0190	LINER
IGR J04085-6546	PESSTO	–	–	–		Sy 1?
IGR J06075-6148	6dF	−0.014	−0.350	2.88	0.0040	LINER
IGR J06503-7742	6df	0.057	0.511	12.64	0.0373	LINER
IGR J08297-4250	X-shooter	–	–	–		Blazar/BL Lac?
IGR J11275-5319	X-shooter	1.01	−0.062	3.58	0.0503	Sy 2
IGR J13045-5630 [(a)]	X-shooter	0.91	−0.140	5.00	0.0511	Sy 2
PKS 1413-36	X-shooter	1.00	−0.313	3.75	0.0753	Sy 2
IGRJ16560-4958 [(a)]	X-shooter	1.20	0.460	>10.77	0.0586	Sy 2
IGR J17255-4509 [(a)]	X-shooter	0.80	0.002	10.40	0.0197	LINER
SWIFT J1839.1-5717	X-shooter	–	–	–	–	Blazar/BL Lac?
SWIFT J1937.5-4021	X-shooter	1.36	0.400	8.59	0.0740	Sy 2

Notes. [(a)]For this source we report the redshift estimate for the first time.

As we mentioned, three objects deserve more in-depth discussion, as their optical spectra are somehow different from that expected from an emission line AGN. The first source is IGR J04085-6546, associated with LEDA 310383. Although the diagnostics all point to an AGN, this source has been associated with a transient event (OGLE 2013-SN-90) occurring on October 6, 2013 (Wyrzykowski et al. 2013), originating from a galaxy, and lasting several months. The follow-up PESSTO observation confirmed the AGN class of the event (Spiro et al. 2013) despite the source photometric class pointing to a type I supernovae (Wyrzykowski et al. 2014). The XRT observation used for this work was performed on Jan 3, 2013, after the peak of the transient event, while the INTEGRAL measurements are the average of multi-year observations. Our analysis of the PESSTO spectrum shows the presence of broad H$_\alpha$ and H$_\beta$ emissions and possibly a narrow [OIII]λ5007 emission line at a redshift $z = 0.116 \pm 0.001$. However, since the spectrum was acquired about one month after the announcement of the OGLE transient, we cannot exclude a contribution from it, especially in the H$_\beta$ region. Nevertheless, we suggest a Seyfert 1 AGN classification for this source.

Another source of interest is IGR J08297-4250. In this case, the low S/N X-shooter spectrum does not allow us to infer the nature of the source. However, the absence of emission and absorption lines, especially at $z = 0$, suggests this source is not a Galactic object. The fact that the radio morphology of the source is core plus jet-like (see Sect. 4.1 and Fig. C.1, right) and seems to point to a BL Lac class. The absence of emission lines in the optical spectra further validates this hypothesis, and we therefore suggest that IGR J08297-4250 is a BL Lac with unknown redshift. Although it is difficult to discriminate blazars from other AGN types simply on the basis of two mid-IR colours, this becomes possible with the use of the three-dimensional WISE colour space, where a third colour, $W3 - W4$, is also used (e.g., Fig. 6 in D'Abrusco et al. 2019). This additional information also allows for discrimination between blazar types (i.e. BL Lacs from flat-spectrum radio quasars). In the case of IGR J08297-4250, $W3 - W4$ is 2.56, which locates the source in the blazar region and well inside the BL Lac locus.

A more controversial case is that of SWIFT J1839.1-5717. Also for this source no emission lines were detected in the optical spectrum, suggesting a similar classification to IGR J08297-4250. However, we noticed that Koss et al. (2022), using the same optical spectrum, classified this source as a Galactic object (i.e. a star) due to the detection of a CaII absorption line. The object is located well below the Galactic plane, it has WISE colours typical of an AGN and not of a stellar object, and its optical spectrum is characterised by a smooth continuum with no apparent absorption lines at redshift $z = 0$. This gives us confidence to rule out the stellar nature for SWIFT J1839.1-5717, and given the above results, we also suggest classification of the source as an AGN and, more specifically, as a BL Lac.

5. Discussion and conclusions

In this work, we have added 83 objects overall to the previous INTEGRAL list of AGN. More than 40% of these objects are in the zone of avoidance, that is, behind our Galaxy where INTEGRAL/IBIS exposure is much deeper than *Swift*/BAT. This peculiarity makes the extragalactic nature of these objects more difficult to establish. Indeed, most of the 34 objects (~68%) listed as AGN in Table A.1 and not classified in the literature, are on the Galactic plane. For these 34 still unclassified sources, we used three diagnostics based on far-IR data, radio detection, and redshift measurement (position in the sky or extension in the optical images) in order to confirm their AGN nature. At least two diagnostics were verified for all 34 candidates, and therefore we can consider them to be AGN, although of unknown class. We were also able to classify 12 AGN among this set of 34 candidates on the basis of publicly available optical spectra, finding that five of them are Seyfert 2 galaxies, four are LINERs, one is a possible Seyfert 1 galaxy (IGR J04085-6546), and two sources are possible BL Lac blazars (IGR J08297-4250 and SWIFT J1839.1-5717). Due to their still uncertain optical classes, we consider the last three objects AGN candidates. Notably, the hard X-ray selection samples all types of AGN, including those of low luminosity. Indeed, our sample lists six BL Lac objects (plus two possible), six flat-spectrum radio quasars, one Narrow Line Seyfert 1 galaxy, five LINERs, two X-ray bright optically normal galaxies (XBONG), 18 Seyfert 1–1.5, and 21 Seyfert 1.8–2.

As previously observed by Malizia et al. (2012), optical classification is generally reflected in the X-ray absorption properties of sources. That is, type 1 objects and blazars are generally unabsorbed, while type 2 sources are either mildly or heavily absorbed. A useful tool to identify outliers to this trend is the diagnostic diagram shown in Fig. 4, as presented in Malizia et al. (2007), where the source column density is plotted against the soft to hard X-ray flux ratio (see Malizia et al. 2007 for a full

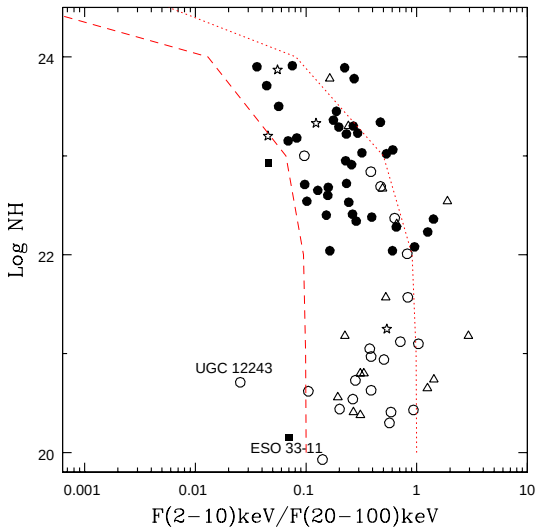

Fig. 4. Log NH versus $F_{2-10\,\mathrm{keV}}/F_{20-100\,\mathrm{keV}}$ flux ratio for our sample sources. Open circles are Seyfert 1–1.5 sources, while filled circles are Seyfert 2 sources. Triangles are blazars, filled squares are XBONG, and stars are LINERs. As in Malizia et al. (2007), lines correspond to the expected values for an absorbed power law with photon index 1.5 (dotted line) and 1.9 (dashed line).

description of this diagnostic). Through this plot, a clear trend of a decreasing softness ratio as the absorption increases is visible, as expected if the 2–10 keV flux is progressively depressed as the absorption becomes stronger. Outliers could be absorbed type 1 AGN with column densities above 10^{22} cm^{-2}, strongly variable sources (Seyfert/blazar) where the soft and hard X-ray fluxes are not simultaneously measured, and Compton thick objects where the column density is not properly estimated. Using the entire INTEGRAL AGN sample, we found that these outliers are approximately 10% of the whole sample; some objects belonging to each class of these outliers have already been pinpointed and extensively discussed in previous works (see for example Malizia et al. 2007, 2009a, 2012).

Most of the sources in the present sample follow the expected trend, except for a few absorbed type 1 AGN (Seyfert 1–1.5 and blazars with column densities above 10^{22} cm^{-2}) that fall in the region populated by absorbed objects. Their peculiarity may be due to either an incomplete account of the Galactic absorption, especially in the AGN located behind the Galactic plane (e.g., the two blazars 4C 50.11 and 4C 39.35), or poor quality of the X-ray spectrum (e.g., for Fairall 1203). Regarding NGC 2617 and MKN 817, the unexpected absorption is likely due to their spectral complexity. For instance, NGC 2617 is a changing-look AGN with a complex X-ray absorption structure and a complex broad-line region (Giustini et al. 2017; Yang et al. 2021). The case of MKN 817 is also quite peculiar, since its absorption is likely ionised and variable and probably interferes with the source disc-corona coupling (Miller et al. 2021). A further anomalous case is that of AX J2254.7+1146(2)/UGC 12243, which as already discussed is a type 1 AGN with no absorption but with a very low soft-to-hard X-ray flux ratio. This could be due to strong variability in the high-energy emission such that combining soft and hard X-ray data not taken contemporaneously provides a false value of the flux ratio. However, a comparison between XRT and XMM observations taken a few years apart does not indicate a change in the source flux within the errors. For this reason, the source may have a highly absorbed soft X-ray spectrum that if not properly corrected for the true column density value, again provides a wrong estimate of the flux ratio. In support of this last hypothesis, we note that Oh et al. (2022) classify UGC 12243 as a type 2 AGN, contrary to previous claim that it is a Seyfert 1 (Véron-Cetty & Véron 2010). If this is true, then UGC 12243 could be another local Compton thick AGN, but in order to understand the true nature of this source, good quality X-ray observations are clearly needed. As expected and visible in Fig. 4, none of the Seyfert 2 are unabsorbed, although the column density in several sources is often quite mild for a type 2 AGN.

Interestingly we did not find any Compton thick AGN, though we would have expected a few. Following Malizia et al. (2009b), 7% of objects below redshift 0.335 are expected to be Compton thick (i.e. around five sources in our sample). More accurately, Torres-Albà et al. (2021) estimate the fraction of Compton thick objects with redshift below 0.05 to be 7.7%, or two to three objects in our case. This further confirms that at high energies, absorption can also prevent the detection of some heavily obscured sources, as first reported in Malizia et al. (2009b). However, the diagnostic plot in Fig. 4 shows a couple of objects with softness ratio values that are too low for the observed column densities, suggesting for them a Compton-thick nature. These objects are UGC 12243 (already discussed above) and the XBONG source IGR J05048-7340/ESO 33-11. In the case of the latter, the optical classification as a normal galaxy could be due to the nuclear emission being completely hidden by the absorption; in addition, it must always be kept in mind that the poor quality of the X-ray spectral data can cause a wrong estimate of the X-ray column density. Nonetheless, this is another interesting source that deserves more in-depth study.

The only Narrow Line Seyfert 1 reported in the sample is RX J1317.0+3735 (Rakshit et al. 2017), which is so far a poorly studied AGN. Its black hole mass is log (M_{BH}) = 6.88, while its Eddington ratio based on the 5100 Å monochromatic luminosity is log Edd = -0.53 (Liu et al. 2019), confirming that this class of AGN tends to have small black hole masses and high Eddington ratios (Rakshit et al. 2017).

Five objects in the present sample are classified as LINERs, and two (IGR J16246-4556 and IGR J16459-2325) are likely to be LINER candidates. Most of these objects display narrow lines and can therefore be classified as type 2 AGN, while only one, IGR J17255-4509, likely belongs to the type 1 class. Their hard X-ray luminosities range from 2×10^{41} erg s^{-1} to a few 10^{43} erg s^{-1}. However, a couple of the objects, despite occupying the lower part of the luminosity versus redshift diagram (see Fig. 1), cannot be considered low-luminosity AGN due to their high luminosity. In addition, the Eddington ratios, available for only a few objects, fall in the range of 0.001–0.009 (Caramete & Biermann 2010), again indicating a behaviour much more similar to Seyfert galaxies. We conclude that the hard X-ray emitting LINERs are definitely active galaxies, but whether their nucleus is similar or different from more canonical AGN is still unclear. Finally, we note that the WISE colour-colour diagram could be used to discriminate between LINERs and other AGN-like Seyferts and blazars, as amply discussed in Sect. 4.1.

Of the reported blazars, nearly all are MeV emitters detected by *Fermi*/LAT, and the only exceptions are IGR J01036-6439, IGR J04426-0018(2), and SWIFT J0600.7+0008. Four blazars (SWIFT J0710.5+5908, RX J1136.5+6737, IGR J20596+4303, and 1ES 2344+514) are also detected at very high energies, TeV. All of these are high-frequency peaked BL Lac. Neither of the two blazar candidates is a *Fermi* source.

In this work, we have added to the INTEGRAL AGN catalogue 83 new sources. Of these sources, more than 40% are located behind the Galactic plane. This fact highlights the importance of INTEGRAL/IBIS in discovering new hard X-ray emitting AGN, mainly in the zone of avoidance where it is much more difficult to discriminate between Galactic and extragalactic objects. The Galactic plane location of the sources makes the multi-waivelength follow-up harder, especially in the UV and optical bands, thus highlighting the importance of also using multiple diagnostic tests to properly classify each object. In this paper, we have shown that WISE colours, radio emission, and morphological evidence can be used as powerful diagnostic tests to identify AGN candidates amongst high-energy emitters.

Acknowledgements. The authors acknowledge financial support from ASI under contract n. 2019-35-HH.0. This research has made use of the NASA/IPAC Extragalactic Database (NED) and NASA/IPAC Infrared Science Archive, which are operated by the Jet Propulsion Laboratory, California Institute of Technology, under contract with the National Aeronautics and Space Administration. This work made use of observations collected at the European Southern Observatory under ESO programs 0103.A-0521(A), 0102.D-0918(A), 0102.A-0433(A), and 0101.A-0765(A). The authors thank the anonymous referee for the useful comments.

References

Ajello, M., Angioni, R., Axelsson, M., et al. 2020, ApJ, 892, 105
Annuar, A., Alexander, D. M., Gandhi, P., et al. 2020, MNRAS, 497, 229
Antonucci, R. 1993, ARA&A, 31, 473
Barthelmy, S. D., Barbier, L. M., Cummings, J. R., et al. 2005, Space Sci. Rev., 120, 143
Bassani, L., Landi, R., Campana, R., et al. 2009, MNRAS, 395, L1
Bird, A. J., Barlow, E. J., Bassani, L., et al. 2004, ApJ, 607, L33
Bird, A. J., Barlow, E. J., Bassani, L., et al. 2006, ApJ, 636, 765
Bird, A. J., Bazzano, A., Malizia, A., et al. 2016, ApJS, 223, 15
Britt, C. T., Strader, J., Chomiuk, L., et al. 2017, ApJ, 849, 21
Burlon, D., Ajello, M., Greiner, J., et al. 2011, ApJ, 728, 58
Caramete, L. I., & Biermann, P. L. 2010, A&A, 521, A55
Chang, Y. L., Arsioli, B., Giommi, P., Padovani, P., & Brandt, C. H. 2019, A&A, 632, A77
Charlot, P., Jacobs, C. S., Gordon, D., et al. 2020, A&A, 644, A159
Clavel, M., Tomsick, J. A., Hare, J., et al. 2019, ApJ, 887, 32
Condon, J. J., Cotton, W. D., Greisen, E. W., et al. 1998, AJ, 115, 1693
D'Abrusco, R., Álvarez Crespo, N., Massaro, F., et al. 2019, ApJS, 242, 4
Edelson, R., & Malkan, M. 2012, ApJ, 751, 52
Fabian, A. C. 2012, ARA&A, 50, 455
Gandhi, P., Yamada, S., Ricci, C., et al. 2015, MNRAS, 449, 1845
Giustini, M., Costantini, E., De Marco, B., et al. 2017, A&A, 597, A66
Gordon, Y. A., Boyce, M. M., O'Dea, C. P., et al. 2021, ApJS, 255, 30
Heckman, T. M., & Best, P. N. 2014, ARA&A, 52, 589
Helfand, D. J., Becker, R. H., White, R. L., Fallon, A., & Tuttle, S. 2006, AJ, 131, 2525
Herpich, F., Mateus, A., Stasińska, G., Cid Fernandes, R., & Vale Asari, N. 2016, MNRAS, 462, 1826
Hickox, R. C., & Alexander, D. M. 2018, ARA&A, 56, 625
Ho, L. C., Filippenko, A. V., & Sargent, W. L. W. 1993, ApJ, 417, 63
Jarrett, T. H., Cluver, M. E., Magoulas, C., et al. 2017, ApJ, 836, 182
Kamraj, N., Brightman, M., Harrison, F. A., et al. 2022, ApJ, 927, 42
Kara, E., Mehdipour, M., Kriss, G. A., et al. 2021, ApJ, 922, 151
Karasev, D. I., Sazonov, S. Y., Tkachenko, A. Y., et al. 2020, Astron. Lett., 45, 836
Kauffmann, G., Heckman, T. M., Tremonti, C., et al. 2003, MNRAS, 346, 1055
Kennedy, M. R., Breton, R. P., Clark, C. J., et al. 2020, MNRAS, 494, 3912
Kormendy, J., & Ho, L. C. 2013, ARA&A, 51, 511
Koss, M. J., Trakhtenbrot, B., Ricci, C., et al. 2022, ApJS, 261, 6
Krivonos, R., Revnivtsev, M., Lutovinov, A., et al. 2007, A&A, 475, 775
Krivonos, R., Tsygankov, S., Lutovinov, A., et al. 2012, A&A, 545, A27
Krivonos, R. A., Tsygankov, S. S., Mereminskiy, I. A., et al. 2017, MNRAS, 470, 512
Krivonos, R. A., Sazonov, S. Y., Kuznetsova, E. A., et al. 2022, MNRAS, 510, 4796
Landi, R., Malizia, A., Bazzano, A., et al. 2011, ATel, 3178, 1
Landi, R., Bassani, L., Bazzano, A., et al. 2017, MNRAS, 470, 1107
Liao, S.-L., Qi, Z.-X., Guo, S.-F., & Cao, Z.-H. 2019, Res. Astron. Astrophys., 19, 029
Liu, H.-Y., Liu, W.-J., Dong, X.-B., et al. 2019, ApJS, 243, 21
Mainzer, A., Bauer, J., Cutri, R. M., et al. 2014, ApJ, 792, 30
Malizia, A., Landi, R., Bassani, L., et al. 2007, ApJ, 668, 81
Malizia, A., Stephen, J. B., Bassani, L., et al. 2009a, MNRAS, 399, 944
Malizia, A., Bassani, L., Panessa, F., de Rosa, A., & Bird, A. J. 2009b, MNRAS, 394, L121
Malizia, A., Bassani, L., Bazzano, A., et al. 2012, MNRAS, 426, 1750
Malizia, A., Molina, M., Bassani, L., et al. 2014, ApJ, 782, L25
Malizia, A., Landi, R., Molina, M., et al. 2016, MNRAS, 460, 19
Malizia, A., Bassani, L., Stephen, J. B., Bazzano, A., & Ubertini, P. 2020a, A&A, 639, A5
Malizia, A., Sazonov, S., Bassani, L., et al. 2020b, New A Rev., 90, 101545
Marchesini, E. J., Paggi, A., Massaro, F., et al. 2020, A&A, 638, A128
Marocco, F., Eisenhardt, P. R. M., Fowler, J. W., et al. 2021, ApJS, 253, 8
Mauch, T., Murphy, T., Buttery, H. J., et al. 2003, MNRAS, 342, 1117
McConnell, D., Sadler, E. M., Murphy, T., & Ekers, R. D. 2012, MNRAS, 422, 1527
McConnell, D., Hale, C. L., Lenc, E., et al. 2020, PASA, 37, e048
Miller, J. M., Zoghbi, A., Reynolds, M. T., et al. 2021, ApJ, 911, L12
Mingo, B., Watson, M. G., Rosen, S. R., et al. 2016, MNRAS, 462, 2631
Molina, M., Malizia, A., Masetti, N., et al. 2021, MNRAS, 507, 3423
Monroe, T. R., Prochaska, J. X., Tejos, N., et al. 2016, AJ, 152, 25
Murphy, T., Mauch, T., Green, A., et al. 2007, MNRAS, 382, 382
Netzer, H. 2015, ARA&A, 53, 365
Oh, K., Koss, M., Markwardt, C. B., et al. 2018, ApJS, 235, 4
Oh, K., Koss, M. J., Ueda, Y., et al. 2022, ApJS, 261, 4
Pushkarev, A. B., & Kovalev, Y. Y. 2012, A&A, 544, A34
Rahoui, F., Tomsick, J. A., & Krivonos, R. 2017, MNRAS, 465, 1563
Rakshit, S., Stalin, C. S., Chand, H., & Zhang, X.-G. 2017, ApJS, 229, 39
Ramos Almeida, C., & Ricci, C. 2017, Nat. Astron., 1, 679
Revnivtsev, M. G., Sunyaev, R. A., Varshalovich, D. A., et al. 2004, Astron. Lett., 30, 382
Revnivtsev, M. G., Sazonov, S. Y., Molkov, S. V., et al. 2006, Astron. Lett., 32, 145
Ricci, C., Ueda, Y., Koss, M. J., et al. 2015, ApJ, 815, L13
Ricci, C., Trakhtenbrot, B., Koss, M. J., et al. 2017, ApJS, 233, 17
Ricci, F., Treister, E., Bauer, F. E., et al. 2022, ApJS, 261, 8
Rodriguez, J., Bodaghee, A., & Tomsick, J. A. 2010, ATel, 2557, 1
Saxton, R. D., Read, A. M., Esquej, P., et al. 2008, A&A, 480, 611
Schlafly, E. F., Green, G. M., Lang, D., et al. 2018, ApJS, 234, 39
Secrest, N. J., Dudik, R. P., Dorland, B. N., et al. 2015, ApJS, 221, 12
Spiro, S., Turatto, M., Benetti, S., et al. 2013, ATel, 5537, 1
Strader, J., Li, K.-L., Chomiuk, L., et al. 2016, ApJ, 831, 89
Tomsick, J. A., Bodaghee, A., Chaty, S., et al. 2012, ApJ, 754, 145
Tomsick, J. A., Krivonos, R., Rahoui, F., et al. 2015, MNRAS, 449, 597
Tomsick, J. A., Bodaghee, A., Chaty, S., et al. 2020, ApJ, 889, 53
Tomsick, J. A., Coughenour, B. M., Hare, J., et al. 2021, ApJ, 914, 48
Torres-Albà, N., Marchesi, S., Zhao, X., et al. 2021, ApJ, 922, 252
Ubertini, P., Lebrun, F., Di Cocco, G., et al. 2003, A&A, 411, L131
Véron-Cetty, M. P., & Véron, P. 2010, A&A, 518, A10
Voges, W., Aschenbach, B., Boller, T., et al. 1996, IAU Circ., 6420, 2
Wyrzykowski, L., Udalski, A., Kozlowski, S., & Skowron, J. 2013, ATel, 5488, 1
Wyrzykowski, Ł., Kostrzewa-Rutkowska, Z., Kozłowski, S., et al. 2014, Acta. Astron., 64, 197
Yamada, S., Ueda, Y., Tanimoto, A., et al. 2021, ApJS, 257, 61
Yang, J., Paragi, Z., Beswick, R. J., et al. 2021, MNRAS, 503, 3886
Zhao, X., Marchesi, S., Ajello, M., et al. 2021, A&A, 650, A57

Appendix A: New INTEGRAL/IBIS AGN

Table A.1. INTEGRAL/IBIS AGN

Name	altern. name	RA	dec	z	class	Log N_H	$\Gamma_{2-10\ keV}$	$F_S^\dagger$	$F_H^\ddagger$	Ref.
SWIFT J0001.6-7701	Fairall 1203	00 01 46.08	−76 57 14.3	0.058	Sy 1	$22.69^{+0.10}_{-0.10}$	1.8 (fixed)	3.39	0.72	1 (XRT)
NGC 235A	-	00 42 52.81	−23 32 27.7	0.022	Sy 2	$23.71^{+0.06}_{-0.06}$	$1.68^{+0.11}_{-0.10}$	2.10	4.76	2
IGR J00569+6359	3PBC J0056.9+6401	00 57 12.70	+63 59 53.2	0.291	Sy 1.2	$22.37^{+0.07}_{-0.08}$	$1.79^{+0.21}_{-0.25}$	2.40	0.38	3
IGR J01036-6439	PKS 0101-649	01 03 33.74	−64 39 07.7	0.163	Blazar/QSO	**20.41**	$1.66^{+0.08}_{-0.06}$	3.00	1.12	3
IGR J01242+3348	NGC 513	01 24 26.80	+33 47 58.2	0.020	Sy 2	$22.72^{+0.04}_{-0.05}$	$1.47^{+0.07}_{-0.07}$	3.89	1.68	1 (XMM + NuSTAR)
SWIFT J0238.2-5213	ESO 198-24	02 38 19.72	−52 11 32.3	0.045	Sy 1	**20.43**	$1.72^{+0.14}_{-0.11}$	12.9	1.38	3
SWIFT J0250.2+4650	LEDA 2287192	02 50 27.18	+46 47 29.4	0.0210	Sy 2	$22.38^{+0.10}_{-0.09}$	$1.36^{+0.28}_{-0.26}$	6.40	1.63	1 (XRT)
IGR J03574-6602	NGC 1503	03 56 33.14	−66 02 27.6	0.019	AGN	∼23.26	1.8 (fixed)	0.34	0.75	1 (XRT)
SWIFT J0359.7+5058	4C 50.11	03 59 29.75	+50 57 50.2	1.520	Blazar/QSO	$22.67^{+0.12}_{-0.10}$	$1.47^{+0.20}_{-0.07}$	5.40	1.10	3
IGR J04059+5416	2MASX J04055765+5418446	04 05 57.66	+54 18 44.7	–	AGN	$22.54^{+0.23}_{-0.34}$	$1.50^{+0.90}_{-0.80}$	1.10	1.08	4
IGR J04085-6546	LEDA 310383	04 08 38.82	−65 45 59.1	0.125	AGN	**20.56**	$1.63^{+0.31}_{-0.30}$	1.31	0.67	1 (XRT)
SWIFT J0414.8-0754	LEDA 14727	04 14 52.66	−07 55 39.7	0.038	Sy 1	**20.73**	$1.97^{+0.92}_{-0.27}$	5.00	1.79	3
NGC 1566	-	04 20 00.40	−54 56 16.6	0.005	Sy 1	**19.93**	$1.73^{+0.07}_{-0.06}$	3.10	2.20	3
SWIFT J0427.0+0734	2MASS J04270427+0716316	04 27 04.28	+07 16 31.7	0.096	Sy 1	**20.94**	$1.61^{+0.17}_{-0.17}$	4.20	0.83	1 (XRT)
IGR J04288-6702[(1)]	LEDA 299570	04 29 47.48	−67 03 18.9	0.065	Sy 1.5	**20.54**	$1.64^{+0.11}_{-0.11}$	1.78	0.68	1 (XRT)
IGR J04426-0018[(2)]	1RXS J044229.8-001823	04 42 30.18	−00 18 29.1	0.449	Blazar/BL Lac	**20.80**	$1.83^{+0.07}_{-0.07}$	1.39	0.42	1 (XRT)
IGR J04426-0018[(2)]	PKS 0440-003	04 42 38.59	−00 17 42.6	0.845	Blazar/QSO	**20.80**	$1.92^{+0.09}_{-0.09}$	1.32	0.42	1 (XRT)
IGR J05048-7340	ESO 33-11	05 05 06.27	−73 39 04.6	0.014	XBONG	**20.15**	$1.8^{+0.3}_{-0.3}$	0.33	0.47	1 (XRT)
IGR J05162-1034	MCG-02-14-009	05 16 21.22	−10 33 41.4	0.029	Sy 1	**20.97**	$2.23^{+0.05}_{-0.05}$	4.20	1.08	3
IGR J05511-1218	LEDA 148076	05 51 13.12	−12 14 42.1	0.035	XBONG	$22.93^{+0.32}_{-0.24}$	1.8 (fixed)	0.8	<1.75	1 (XRT), 5, 6
SWIFT J0600.7+0008	IRAS05581+0006	06 00 40.11	+00 06 18.4	0.115	Sy 1.9	$23.30^{+0.11}_{-0.11}$	1.8 (fixed)	1.99	0.83	1 XRT
IGR J06075-6148	ESO 121-6	06 07 29.85	−61 48 27.3	0.004	AGN	$23.33^{+0.03}_{-0.03}$	$1.89^{+0.08}_{-0.08}$	0.95	0.73	7
IGR J06380-7536	LEDA 243576	06 37 43.17	−75 38 46.3	0.089	Sy 1.8	–	–	–	0.78	no (2-10) data
IGR J06503-7742⋆	LEDA 235040	06 49 54.37	−77 42 18.6	0.037	AGN	–	–	0.64	0.94	8
IGR J07072-1227	2MASX J07071126-1227560	07 07 11.43	−12 28 00.2	0.071	Sy 2	$22.71^{+0.56}_{-0.35}$	1.8 (fixed)	1.11	1.13	1 (XRT), 5
SWIFT J0710.5+5908	RX J0710.5+5908	07 10 30.07	+59 08 20.3	0.125	Blazar/BL Lac	**20.65**	$1.80^{+0.04}_{-0.04}$	28.5°	2.28	1 (XRT)
IGR J07328-4640	PKS 0731-465	07 32 44.31	−46 40 17.2	–	Blazar/QSO	$21.18^{+0.20}_{-0.28}$	1.8 (fixed)	1.99	0.89	1 (XRT)
RX J0818.9-2252	LEDA 80921	08 18 57.72	−22 52 36.2	0.035	Sy 1	**21.05**	$1.79^{+0.09}_{-0.09}$	3.46	0.93	1 (XRT)
SWIFT J0823.4-0457	Fairall 272	08 23 01.10	−04 56 05.4	0.022	Sy 2	$23.23^{+0.05}_{-0.05}$	$1.51^{+0.11}_{-0.08}$	6.46	2.22	9
IGR J08297-4250	2MASX J08294112-4251582	08 29 41.12	−42 51 58.3	–	AGN	$23.78^{+0.43}_{-0.53}$	$1.50^{+0.90}_{-0.80}$	1.10	0.67	4
SWIFT J0835.5-0902[(3)]	2MASX J08353333-0905302	08 35 33.34	−09 05 30.2	0.112♣	AGN	**20.62**	$2.04^{+0.13}_{-0.13}$	1.68	1.62	1 (XRT)
NGC 2617	-	08 35 38.00	−04 05 17.9	0.014	Sy 1/1.8	$23.34^{+0.07}_{-0.08}$	$1.87^{+0.01}_{-0.01}$	23.5	5.00	10
PKS 0921-213	-	09 23 38.88	−21 35 47.1	0.053	Sy 1	**20.63**	$1.77^{+0.08}_{-0.08}$	6.23	1.60	1 (XRT)
SWIFT J0924.2-3142	2MASS J09235373-3141308	09 23 53.61	−31 41 31.6	0.042	Sy 1.8	$23.91^{+0.23}_{-0.27}$	1.8 (fixed)	1.7	2.26	11
SWIFT J0958.2-5732	WISEA J095834.97-572927.2	09 58 35.03	−57 29 26.7	–	AGN	$22.28^{+0.07}_{-0.09}$	1.8 (fixed)	3.44	0.52	1
ESO 317-41	SWIFTJ1031.5-4205	10 31 23.11	−42 31 23.1	0.019*	Sey 2	$23.90^{+0.07}_{-008.}$	$1.76^{+0.31}_{-0.21}$	0.44	1.11	9
IGR J10447-6027	2MASS J10445192-6025115	10 44 51.91	−60 25 11.9	0.047	Sy 2	$23.22^{+0.07}_{-0.07}$	$1.50^{+0.06}_{-0.06}$	2.20	0.95	12
IGR J10595-5125	ESO 215-14	10 59 19.03	−51 26 32.3	0.019	Sy 1	**21.10**	$1.65^{+011.}_{-0.11}$	5.71	0.55	1 (XRT)
IGR J11275-5319	2MASX J11273392-5320270	11 27 33.90	−53 20 25.9	0.049♣	AGN	$23.18^{+0.26}_{-0.22}$	1.8 (fixed)	0.84	0.97	1 (XRT)
IGR J11299-6557	2MASS J11295643-6555218	11 29 56.90	−65 55 18.9	–	AGN	<22.04	$2.09^{+0.98}_{-0.81}$	3.20	0.53	1 (XRT)
RX J1136.5+6737	SWIFT J1136.7+6738	11 36 30.10	+67 37 04.0	0.134	Blazar/BL Lac	$20.74^{+0.09}_{-0.14}$	$2.04^{+0.05}_{-0.04}$	11.6	0.81	3
NGC 4102	-	12 06 23.11	+52 42 39.4	0.003	LINER	$23.87^{+0.04}_{-0.03}$	$1.74^{+0.12}_{-0.08}$	1.44	2.53	9
IGR J12418+7805[4,⋆]	LEDA 140000	12 42 36.10	+78 07 20.4	0.022	Sy 1.9	–	–	1.00	0.94	8
PKS 1252+11	-	12 54 38.25	+11 41 05.9	0.872	Blazar/QSO	**20.38**	$1.30^{+0.48}_{-0.48}$	1.77	0.58	1 (XRT)
IGR J13045-5630	WISE J130431.77-563058.5	13 04 31.50	−56 30 54.8	–	AGN	$23.29^{+0.24}_{-0.28}$	1.8 (fixed)	1.82	0.91	13
RX J1317.0+3735	-	13 17 02.89	+37 35 32.7	0.195	NLS1	–	–		1.02	no (2-10) keV data
ESO 509-G038	-	13 31 13.84	−25 24 09.9	0.026	Sy 1	**20.44**	$1.56^{+0.09}_{-0.09}$	3.44	1.69	1 (XRT)
PKS 1413-36	-	14 16 33.16	−36 40 53.8	0.075	AGN	$22.53^{+0.13}_{-0.11}$	1.8 (fixed)	1.77	0.74	1 (XRT)
MRK 1383	-	14 29 06.57	+01 17 06.1	0.087	Sy 1	**20.41**	$1.87^{+0.02}_{-0.02}$	6.50	1.11	1 (XMM+NuSTAR)
MRK 817	-	14 36 22.08	+58 47 39.4	0.031	Sy 1.2	$22.84^{+0.05}_{-0.04}$	$1.91^{+0.04}_{-0.09}$	6.67	1.74	14
MRK 477	-	14 40 38.09	+53 30 16.2	0.038	Sy 2	$23.30^{+0.06}_{-0.07}$	$1.58^{+0.09}_{-0.07}$	3.38	1.27	9
IGR J14417-5533	WISE J144118.74-553335.1	14 41 18.94	−55 33 33.5	–	AGN	**21.57**	$1.55^{+0.24}_{-0.24}$	7.38	0.89	1 (XRT)
IGR J14557-5448	LEDA 415943	14 55 32.19	−54 46 31.3	–	AGN	$23.15^{+0.17}_{-0.12}$	1.8 (fixed)	0.44	0.58	1 (XMM)
IGR J16005-4645	PMN J1600-4649	16 00 20.40	−46 48 41.3	–	AGN	$22.08^{+0.39}_{-0.51}$	1.8 (fixed)	4.40	0.46	1 (XRT)
3C 332.0	-	16 17 42.54	+32 22 34.4	0.151	Sy 1	$22.01^{+0.17}_{-0.10}$	$1.77^{+0.04}_{-0.04}$	9.22	1.12	1 (XRT + NuSTAR)
IGR J16181-5407	2MASS J16180771-5406122	16 18 07.74	−54 06 12.2	0.085	AGN	$22.95^{+0.25}_{-0.65}$	$0.8^{+1.10}_{-1.10}$	1.27	0.57	15
IGR J16246-4556	2MASS J16243080-4555144	16 24 30.77	−45 55 14.1	–	AGN	$22.40^{+0.21}_{-0.45}$	$1.3^{+0.70}_{-0.07}$	0.93	<0.59	15
IGR J16413-4046	CXOU J164119.4–404737	16 41 19.5	−40 47 37.7	–	AGN	23	1.8 (fixed)	1.40	1.45	16
IGR J16459-2325	ESO 518-2	16 45 54.95	−23 27 05.5	0.020	AGN	∼23.78	1.8 (fixed)	4.30	1.58	1 (XRT)
IGR J16560-4958	CXOU J165551.9–495732	16 55 51.95	−49 57 32.4	–	AGN	$22.36^{+0.07}_{-0.11}$	$2.3^{+0.70}_{-0.40}$	17.00	1.20	17
IGR J17157-5449	2MASS J17153752-5450062	17 15 37.53	−54 50 05.1	–	AGN	**21.12**	$1.51^{+0.15}_{-0.15}$	4.25	0.59	1 (XRT)
IGR J17255-4509	2MASX J17253053-4510279	17 25 30.55	−45 10 27.3	0.019	AGN	$21.25^{+0.24}_{-0.30}$	1.8 (fixed)	2.91	0.54	1 (XRT)
SWIFT J1745.4+2906	1RXSJ174538.1+290823	17 45 38.29	+29 08 22.7	0.111	Sy 1	<20.30	$1.57^{+0.03}_{-0.03}$	7.08	1.25	1 (XRT+ NuSTAR)
IGR J18134-1636	-	18 13 28.03	−16 35 48.5	–	AGN	$22.65^{+0.39}_{-0.33}$	1.8 (fixed)	1.15	0.94	1 (XRT)
IGR J18141-1823	4PBC J1814.1-1822	18 14 14.78	−18 23 09.6	–	AGN	$22.68^{+0.21}_{-0.19}$	1.8 (fixed)	0.98	0.63	1 (XRT)
AX J1830.6-1002	-	18 30 38.3	−10 02 47.1	–	AGN	$23.03^{+0.12}_{-0.13}$	$1.01^{+0.57}_{-0.38}$	3.20	1.00	18

Table A.1. Continued from previous page.

Name	altern. name	RA	dec	z	class	Log N_H	$\Gamma_{2-10\ keV}$	$F_S^{\dagger}$	$F_H^{\ddagger}$	Ref.
IGR J18381-0924	CXOU J183818.5-092552	18 38 18.58	−09 25 52.2	0.031	Sy 1.9	$22.34^{+0.03}_{-0.03}$	$1.19^{+0.07}_{-0.07}$	2.30	0.81	19
SWIFT J1839.1-5717	allWISE J183905.95-571505.1	18 39 06.37	−57 15 05.8	–	AGN	$22.31^{+0.07}_{-0.07}$	$1.57^{+0.21}_{-0.21}$	8.40	1.27	11
IGR J18486-0047	CXOU J184825.4?004635	18 48 25.45	−00 46 34.9	–	AGN	$23.45^{+0.17}_{-0.28}$	1.8 (fixed)	1.63	0.85	1 (XRT)
IGR J18497-0248	NVSS J184946-024819	18 49 46.67	−02 48 17.3	–	AGN	~22.60	1.8 (fixed)	1.08	0.70	1 (XRT)
IGR J19294+1328	CXOU J192930.1+132705	19 29 30.11	+13 27 05.6	–	AGN	$23.89^{+0.25}_{-0.21}$	1.8 (fixed)	1.87	0.85	1(XRT), 14
SWIFT J1937.5-4021[2]	LEDA 588288	19 37 13.47	−40 16 14.8	0.075	AGN	$22.23^{+0.09}_{-0.10}$	$1.51^{+0.25}_{-0.25}$	3.92	0.31	1(XRT)
SWIFT J1937.5-4021[2]	1RXS J193716.1-401026	19 37 14.70	−40 10 14.9	–	AGN	$22.91^{+0.46}_{-0.67}$	$1.92^{+0.21}_{-0.23}$	0.78	0.31	1(XRT)
IGR J19504+3319	2MASS J19501973+3314166	19 50 19.73	+33 14 16.2	–	AGN	$22.04^{+0.14}_{-0.19}$	$1.8^{+0.3}_{-0.3}$	2.24	1.34	20
IGR J19577+3339	CXOU J195740.5+333828	19 57 40.59	+33 38 28.2	–	AGN	<23.5	$-0.6^{+4.5}_{-1.6}$	0.26	0.53	20
IC 5063	-	20 52 02.33	−57 04 07.6	0.011	Sy 2	$23.36^{+0.02}_{-0.02}$	$1.77^{+0.08}_{-0.07}$	8.70	4.92	9
SWIFT J2055.0+3559	2MASS J20550835+3556278	20 55 08.23	+35 56 27.4	0.115♣	AGN	$23.02^{+0.16}_{-0.15}$	1.8 (fixed)	2.50	0.47	1 (XRT)
IGR J20569+4940	4C 49.35	20 56 42.74	+49 40 06.6	0.100♣	Blazar/BL Lac	$22.54^{+0.05}_{-0.05}$	$2.60^{+0.03}_{-0.03}$	22.0	1.16	12
IGR J20596+4303[(5)]	-	21 00 01.00	+43 02 11.0	0.066	Sy 2	$22.41^{+0.11}_{-0.13}$	1.8	1.49	0.57	21
IGR J22018+5049	NRAO 676	22 01 43.54	+50 48 56.4	1.899	Blazar/QSO	**21.57**	$1.39^{+0.07}_{-0.07}$	5.20	0.99	1 (XRT)
AX J2254.3+1146[(2)]	UGC 12237	22 54 19.67	+11 46 56.8	0.0286	Sy 2	$23.06^{+0.14}_{-0.13}$	1.8 (fixed)	3.10	0.51	1 (XRT)
AX J2254.7+1146[(2)]	UGC 12243	22 54 43.51	+11 42 50.9	0.0278	Sy 1	**20.71**	$1.75^{+0.72}_{-0.79}$	0.13	0.51	1 (XRT)
1ES 2344+514	-	23 47 04.84	+51 42 17.9	0.044	Blazar/BL Lac	**21.18**	$1.96^{+0.02}_{-0.02}$	17.0	0.58	1 (XRT)

Notes: Sources in bold are (also) in cat 1000. Values of Log N_H in bold are for sources where only Galactic absorption was measured; for the rest of the sample sources, the Galactic absorption was always considered in addition to the intrinsic one listed; [(†)] 2-10 keV flux in units of 10^{-12} erg cm^{-2} s^{-1}; [(‡)] 20-100 keV flux in units of 10^{-11} erg cm^{-2} s^{-1}. **(1)** Two sources are present within the IBIS error circle: a Seyfert 1 galaxy, whose values are reported in the table, and an eclipsing X-ray binary, a transitional millisecond pulsar (SXPS J042749.2-670434). Both sources were detected above 3 keV; therefore, the hard X-ray emission could be due to the contribution of the two sources. **(2)** Two sources are present within the IBIS error circle, both AGN, and both are reported in the table. The hard X-ray emission could be the result of the contribution of two objects, and therefore the value reported in Krivonos has been divided by two. **(3)** Two sources lie within the IBIS error circle: the galaxy 2MASX J08353333-0905302, with the photometric redshift reported in the table, and a rotationally variable star, ASAS J083531-0904.1. Both objects emit above 5 keV; therefore, they could both contribute to the hard X-ray emission. [(⋆)] For these sources, only the XMM Slew Survey flux is available. **(4⋆)** Two sources are listed in the XMM Slew Survey: LEDA140000 (also ROSAT Bright), reported in the table, and XMMSL2 J124313.8+780828, which is unidentified and has a 2-10 keV flux of 5.9×10^{-12} erg cm^{-2} s^{-1}. Both sources probably contribute to the high-energy emission. **(5)** Two sources lie within the IBIS error circle. One is the Seyfert 2 reported in the table, while the second is a CV. They both contribute to the high-energy flux. ◦ Mean value. ♣ Photometric redshift. * Redshift and optical class from Oh et al. (2022).
References: 1): This work; 2): Yamada et al. (2021); 3): Ricci et al. (2017); 4): Tomsick et al. (2015); 7): Annuar et al. (2020); 8) Saxton et al. (2008); 9) Zhao et al. (2021); 10) Giustini et al. (2017); 11) Landi et al. (2017); 12) Clavel et al. (2019); 13) Rodriguez et al. (2010); 14) Kara et al. (2021); 15) Tomsick et al. (2020); 16) Landi et al. (2011); 17) Tomsick et al. (2012) 18) Bassani et al. (2009); 19) Rahoui et al. (2017); 20) Tomsick et al. (2021) 21) Karasev et al. (2020)

Appendix B: Swift/XRT fields of multiple counterparts

In this appendix, the Swift/XRT fields of peculiar sources where multiple counterparts have been found and discussed in Section 3 are shown. To better visualise and highlight the X-ray counterparts of the new INTEGRAL AGN, the images were smoothed. Therefore, the presence of grains and/or features inside the XRT field of view are undoubtedly spurious.

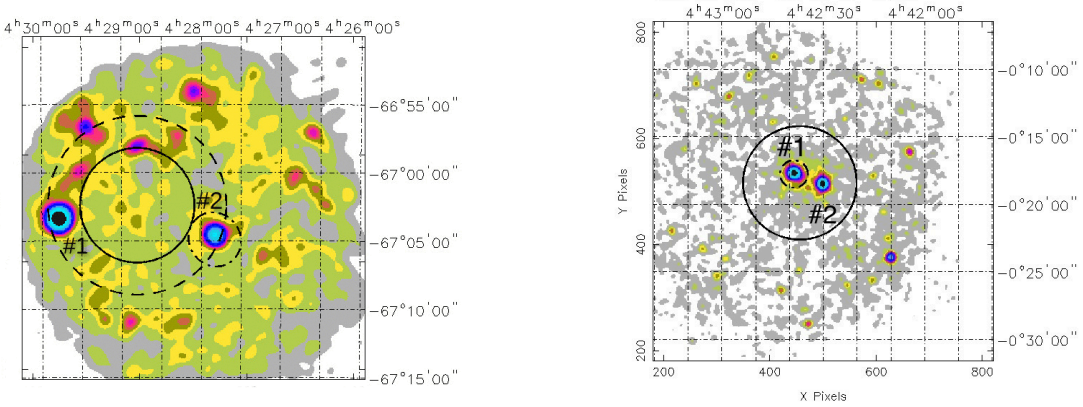

Fig. B.1. Swift/XRT images. Left: 0.3-10 keV band image of IGR J04288-6702 also SWIFT J0428.2-6704. The two X-ray counterparts are inside the 99% IBIS positional uncertainty (dashed circle). Source #1 is the Seyfert 1.5 LEDA 299570 at z=0.065, while source #2 is SXPS J042749.2-670434, the eclipsing low-mass X-ray binary also detected in the Fermi/LAT catalogue (error ellipse). Right: 0.3-10 keV band image of PKS 0441-0017 (source #1) and 1RXS J044229.8-001823 (source #2), both well inside the 90% IBIS error circle. The small dashed-dotted ellipse corresponds to the Fermi/LAT positional error of 4FGL J0442.6-0017.

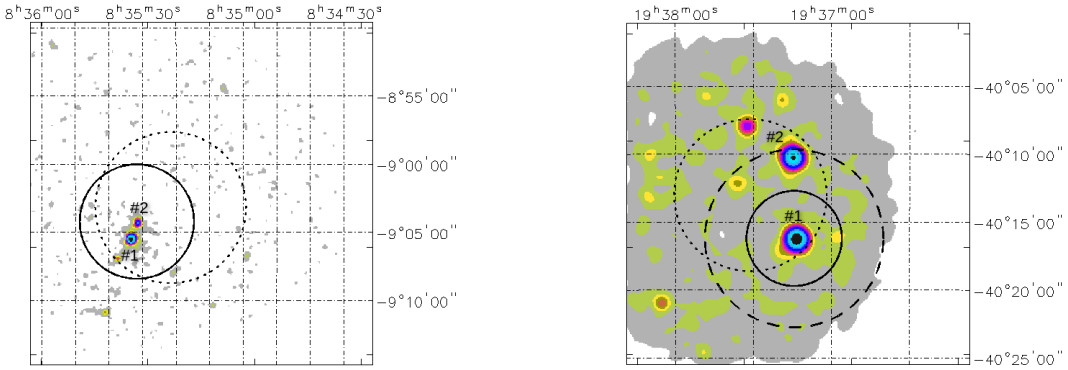

Fig. B.2. Swift/XRT images. Left: 0.3-10 keV band of SWIFT J0835.5-0902. Two X-ray counterparts are well inside the IBIS (continuous circle) and BAT (dotted circle) error circles. Source #1 is the AGN candidate 2MASX J08353333-0905302, while source #2 is associated with the variable star ASAS J083531-0904.1. Right: 0.3-10 keV image of SWIFT J1937.5-4021. Source #1, which lies inside the IBIS (continuous circle) and BAT (dotted circle) and has a 90% positional uncertainty, is the Seyfert 2 LEDA 5882882. Source #2, which is well inside the BAT error circle, is instead located inside the 99% IBIS positional uncertainty (dashed circle), and it is associated with 1RXS J193716.1-401026.

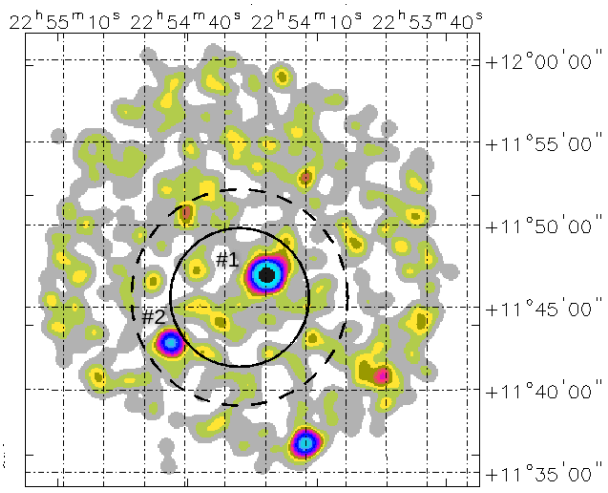

Fig. B.3. Swift/XRT 0.3-10 keV image of AX J2254.3+1146, also called SWIFT J2254.2+1147. Two likely counterparts were detected in X-rays. Source #1, which falls within the 90% IBIS positional uncertainty (filled circle) is the Seyfert 2 UGC 12237, while source #2, which was detected within the 99% IBIS error circle (dashed circle), is the Seyfert 1 UGC 12243.

Appendix C: Radio images of resolved AGN candidates

The radio images of the resolved sources discussed in Section 4.1 are shown in Figures C.1 and C.2. For IGR J19577+3339, only VLASS imges are available, while for IGR J08297-4250 and IGR J16005-4645 RACS images are available. For the radio galaxy PKS 1413-36, both VLASS and RACS images could be retrieved. With a resolution of ~2.5 arcsec and an average RMS of ~0.120 mJy/beam, VLASS is more sensitive to compact features (<1 arcmin), but RACS at a resolution of 25 arcsec and average RMS of ~0.25 mJy/beam is able to recover extended emission up to ~1 deg.

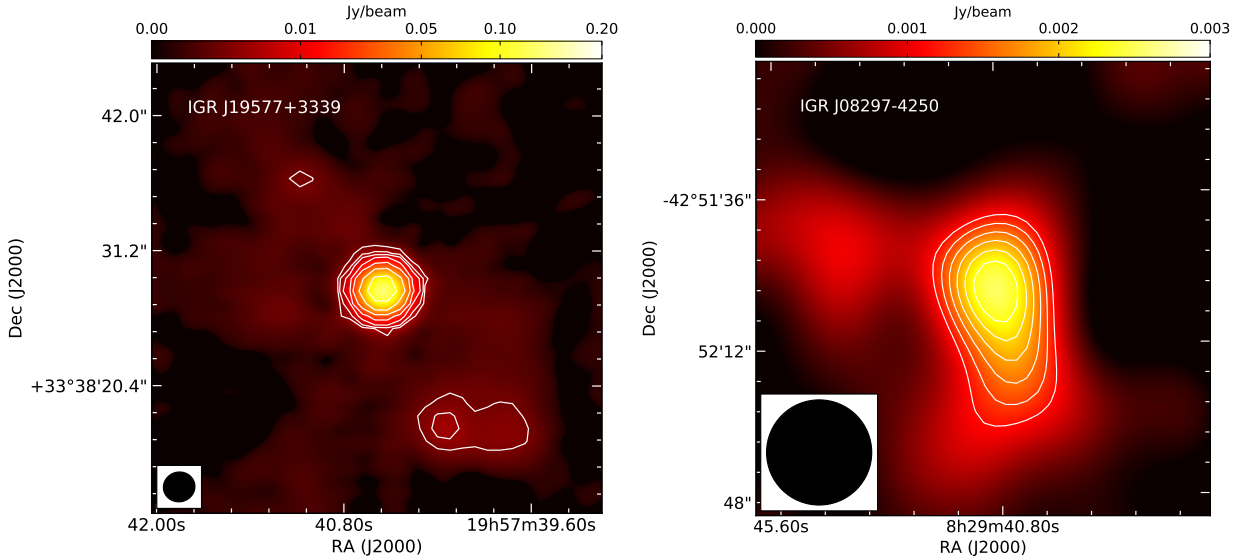

Fig. C.1. Radio images. Left panel: VLASS image of source IGR J19577+3339. Contours are 3×RMS×(1,2,4,8,16,32,64). Right panel: RACS image of source IGR J08297-4250. Contours are RMS×(5,6,7,8,9,10). The angular resolution is shown in the lower-left corner.

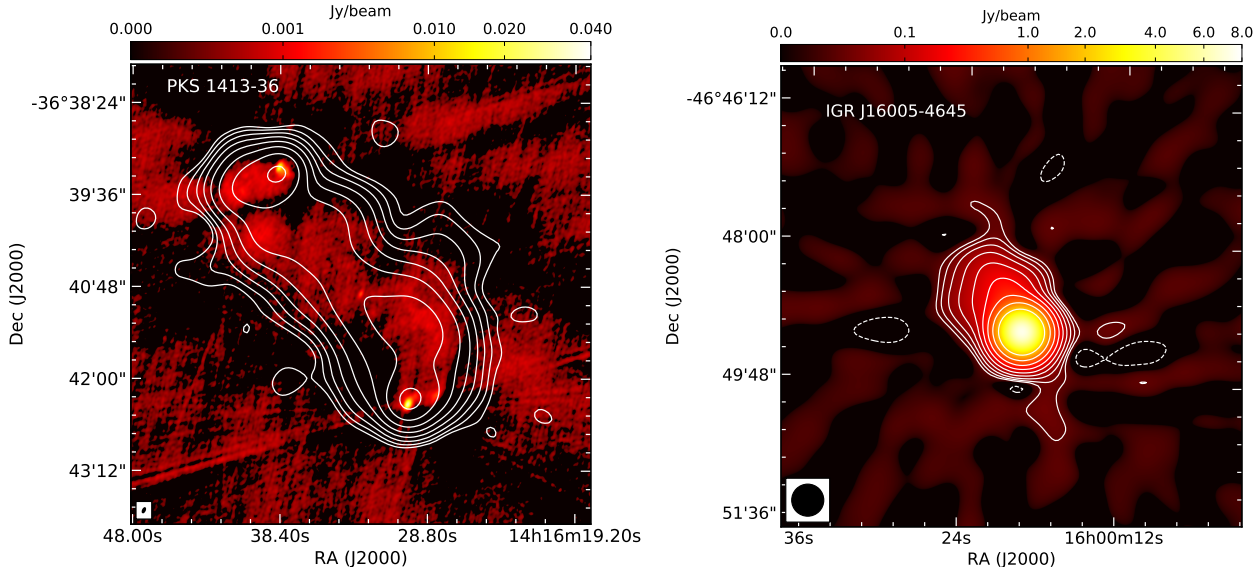

Fig. C.2. Radio images. Left panel: VLASS image of source PKS 1413-36 with overlayed contours from RACS corresponding to 3×RMS×(1,2,4,8,16,32,64,128). Right panel: RACS image of source IGR J160005-4645. Contours are 3×RMS×(1,2,4,8,16,32,64,128,256). The angular resolution is shown in the lower-left corner.